

Published in final edited form as:

*Chem Commun (Camb)*. 2012 October 9; 48(78): 9768–9770. doi:10.1039/c2cc31974h.

## A nanoscale graphene oxide–peptide biosensor for real-time specific biomarker detection on the cell surface†

Zhe Wang<sup>a,b,c</sup>, Peng Huang<sup>a,b</sup>, Ashwinkumar Bhirde<sup>b</sup>, Albert Jin<sup>d</sup>, Ying Ma<sup>b</sup>, Gang Niu<sup>b</sup>, Nouri Neamati<sup>c</sup>, and Xiaoyuan Chen<sup>b</sup>

<sup>a</sup>Center for Molecular Imaging and Translational Medicine, School of Public Health, Xiamen University, Xiamen, China 361005

<sup>b</sup>Laboratory of Molecular Imaging and Nanomedicine, National Institute of Biomedical Imaging and Bioengineering, National Institutes of Health, Bethesda, MD 20892, USA. shawn.chen@nih.gov; Fax: +1 301-480-1613; Tel: +1 301-451-4246

<sup>c</sup>Department of Pharmacology and Pharmaceutical Sciences, University of Southern California, School of Pharmacy, Los Angeles, CA 90089, USA. neamati@usc.edu; Fax: +1 323-442-1390; Tel: +1 323-442-2341

<sup>d</sup>Laboratory of Cellular Imaging and Macromolecular Biophysics, National Institute of Biomedical Imaging and Bioengineering, National Institutes of Health (NIH), Bethesda, MD 20892, USA

### Abstract

A nanoscale RGD–pyrene–graphene oxide (GO) biosensor was prepared for real-time *in situ* detection of a cancer cell surface marker, integrin  $\alpha v \beta 3$ . This nanoscale GO-based biosensor is simple, robust, sensitive and of high selectivity. It can also be adapted to other cancer cell surface marker evaluation systems.

With the fast advancement of nanotechnology, many nanomaterials including quantum dots, carbon nanotubes, magnetic nanoparticles, and gold nanoparticles or nanorods *etc.*, have been integrated with biomolecules for advanced biomedical applications, such as drug/gene delivery,<sup>1</sup> bioimaging<sup>2–4</sup> and biosensing.<sup>5</sup> Graphene, a 2D honeycomb lattice consisting of  $sp^2$ -hybridized carbons, has recently drawn much attention due to its distinct electronic, mechanical, optical and thermal properties from other carbon materials for various applications.<sup>6</sup> The oxidized counterpart of graphene, graphene oxide (GO), provides a new type of aqueous dispersible biocompatible material for biological applications. GO has been reported to be an effective drug delivery system to carry poorly water soluble anticancer drugs for cancer therapy.<sup>7,8</sup> Due to the aromatic domain and multiple ionic components of the basal plane, GO bears the unique capacity to absorb biomolecules, such as nucleic acid<sup>9,10</sup> or protein,<sup>11</sup> to behave as a sensitive biosensor. In addition, the  $sp^2$  aromatic domain of GO results in the quenching effect of nascent fluorescent dyes *via* fluorescence resonance energy transfer (FRET) or dipole–dipole coupling effects.<sup>12</sup> This property facilitates GO to serve as a fluorescence quencher for fluorescence “on–off” biosensing.

So far, GO has been employed to detect various biomolecules. Noncovalent binding of GO with dye-labeled single strand DNA (ssDNA) enables efficient detection of target DNA in biological samples.<sup>10</sup> GO can also be combined with dye-tagged peptides to sense protease

†Electronic supplementary information (ESI) available.

activities.<sup>13,14</sup> In addition, the modified GO has been used to sense ATP activity<sup>15,16</sup> and prostate specific antigen (PSA) detection.<sup>17</sup> Although there are many GO based biosensors available, the use of GO as a sensitive biosensor for highly specific cancer cell surface marker detection remains unexplored.

As one of the widely used fluorescent dyes, pyrene possesses large extinction coefficient, high quantum yield, and good stability in aqueous media.<sup>18</sup> Because of these attributes, pyrene has been used as an optical reporter molecule for the detection of infectious prion protein<sup>19</sup> and DNA.<sup>20</sup>

Additionally, pyrene and its derivatives present noncovalent interaction with molecules with a  $\pi$ -electron rich framework, such as GO, carbon nanotubes, and fullerenes.<sup>21</sup> Hence, the combination of GO and pyrene provides an ideal platform for biosensing. In this study, we report a GO-based biosensor to efficiently detect cancer cell surface markers. As a proof-of-principle, we employed cyclic RGD peptide and integrin  $\alpha v \beta 3$  as a ligand–receptor pair for GO based biosensing due to the vital role of integrin in cancer cell adhesion, proliferation, migration and metastasis.<sup>22</sup> This GO based biosensor system is initially at a quenching state due to the proximity of RGD–pyrene to GO upon  $\pi$ -stacking interactions. However, the competitive binding of an RGD receptor, integrin  $\alpha v \beta 3$ , to the RGD ligand disturbs the adsorption of RGD–pyrene onto the GO surface, resulting in the recovery of pyrene fluorescence. In addition to the detection of purified integrin protein in buffer, which is a routinely used method under many biosensor working conditions, we further demonstrated the effectiveness for *in situ* detection of integrin overexpression in live and fixed breast cancer cells.

Scheme 1 illustrates the principle of RGD–pyrene–GO biosensor for sensitive detection of integrin  $\alpha v \beta 3$  in solution or on the cell surface membrane. A head-to-tail cyclic RGD containing peptide, c(RGDyK), was used here due to its high receptor binding affinity.<sup>2,23</sup> The as-synthesized RGD–pyrene conjugate (Fig. S1, ESI†) presents sol–gel character in aqueous solution at concentration 3 mM. For cell surface marker detection, we used a low concentration of this conjugate, 2  $\mu$ M, at which it is well-dispersed in solution. Upon addition of RGD–pyrene into GO solution, the strong interaction of pyrene with the basal plane of GO results in immediate quenching of pyrene fluorescence due to the energy transfer between GO and pyrene. Fig. S2a (ESI†) shows the UV/Vis spectra of RGD–pyrene with GO. It can be seen that the GO peak at 230 nm is slightly shifted to 232 nm in the RGD–pyrene–GO complex, and the absorption peak of RGD–pyrene at 348 nm is shifted to 351 nm. These slight red shifts indicate the  $\pi$ – $\pi$  interaction of pyrene with GO. To investigate the dynamic interaction range of GO with the RGD–pyrene conjugate, the absorption peak values at 232 nm were plotted against the RGD–pyrene–GO complex concentrations (Fig. S2b inset, ESI†). The extinction coefficient of the RGD–pyrene–GO complex was estimated by Beer's law from the slope of linear square fit.<sup>20</sup> It was found to be 0.0088 L mg<sup>-1</sup> cm<sup>-1</sup> with an  $R^2$  value of 0.9996. Fig. S2c (ESI†) shows the fluorescence spectra of RGD–pyrene at different concentrations with an excitation wavelength of 338 nm. The linear relationship between the fluorescence intensity at the 400 nm emission peak and RGD–pyrene concentration (Fig. S2c inset, ESI†) confirms the good dispersion of the GO–RGD–pyrene complex in aqueous solution. The atomic force microscopy (AFM) images shown in Fig. 1 confirm the formation of the GO–peptide complex with good dispersion, and maintenance of the original nanoscale character of GO. The adsorption of RGD–pyrene on GO resulted in 1–1.5 nm increase in thickness, and marginal increase in size (Fig. 1b).

Next, we investigated the quenching effect of GO on the fluorescence of the RGD–pyrene conjugate. Fig. 2 shows the concentration dependent fluorescence quenching effect of GO on RGD–pyrene in aqueous solution. An exponential reduction of RGD–pyrene was

observed with increasing concentration of GO. The quenching efficiency of GO is calculated by using the formula:  $Q_E = (1 - \alpha) \times 100\%$ , where  $\alpha$  is the ratio of fluorescence quenched to the original fluorescence of the RGD–pyrene conjugate. Hence, the  $Q_E$  of GO to the RGD–pyrene conjugate (2  $\mu\text{M}$ ) is calculated to be  $96.2 \pm 0.13\%$ . Higher concentrations of GO did not further quench the fluorescence of pyrene significantly. In the subsequent studies, 2  $\mu\text{M}$  RGD–pyrene and 2  $\mu\text{g mL}^{-1}$  GO were used for integrin biosensing.

In the presence of purified integrin  $\alpha v \beta 3$  in RGD binding buffer (pH 7.4), the fluorescence intensity enhancement of RGD–pyrene–GO was observed (Fig. S3, ESI†). This fluorescence recovery (FR) indicates that the competitive binding of RGD–pyrene with integrin dissociates the  $\pi$ – $\pi$  coupling and hydrophobic interaction of GO with pyrene (Fig. S3a, ESI†), and the recovered fluorescence intensity increased in accordance with the ascending concentrations of integrin in buffer (Fig. S3b, ESI†). To study the binding specificity of this RGD–pyrene probe to integrin  $\alpha v \beta 3$ , we investigated the fluorescence recovery of RGD–pyrene in various biological samples. As shown in Fig. 3, the probe exhibited little FR to nonspecific biological moieties, while the FR of integrin  $\alpha v \beta 3$  to the RGD–pyrene probe was up to 52.3%. This result confirms that the RGD–pyrene probe can be used as a selective fluorescent probe to target the cancer surface marker, integrin  $\alpha v \beta 3$ .

The kinetic behavior of RGD–pyrene with GO was studied by recording the fluorescence intensity as the function of time (Fig. S4, ESI†). Fig. S4a (curve a, ESI†) presents the kinetics of fluorescence quenching of pyrene in the presence of GO over time. The interaction of RGD–pyrene with GO was very fast at room temperature (22 °C), reaching an equilibrium within 1 min. When the RGD–pyrene–GO complex was exposed to integrin, the competitive binding of integrin to the RGD ligand resulted in gradual dissociation of the RGD–pyrene probe from the GO surface, leading to a time-dependent FR. The recovery reached maximum and plateaued after 10 min incubation (Fig. S4, curve b, ESI†). This fast kinetic behavior of RGD–pyrene–GO and integrin enables highly selective and efficient detection of integrin for biosensing.

Next, we applied this RGD–pyrene–GO probe to cancer cells for *in situ* cell surface marker evaluation. We chose the MDA-MB-435 cell line, which was reported to overexpress integrin on the cell surface,<sup>24</sup> and MCF-7 which has very low integrin expression level<sup>25</sup> for comparison. After 2 hour incubation of the probe and corresponding cancer cells, the pyrene fluorescence signal was recovered in the MDA-MB-435 cell culture (Fig. 4a and b, Fig. S6, ESI†), while a negligible fluorescent signal was detected from the MCF-7 cells (Fig. S6 and S8, ESI†). Free c(RGDyK) peptide effectively blocked the recovery of fluorescence in MDA-MB-435 cell culture, which confirmed the specificity of the RGD–pyrene–GO probe (Fig. S6 and S8, ESI†). In contrast, fluorescent RGD–pyrene without GO showed different cellular uptake behavior in which the GO free RGD–pyrene probe diffused into cytoplasm upon integrin binding (Fig. 4c,d and Fig. S6–S8, ESI†) after 2 h incubation. This is partially due to the hydrophobicity of pyrene. In contrast, the RGD–pyrene–GO probe bound to the cell surface membrane (Fig. 4a,b, white arrow, Fig. S6–S8, ESI†). Flow cytometry results (Fig. S5, ESI†) confirmed the above phenomena. This specific cell receptor binding study provides the initial evidence that the RGD–pyrene–GO complex is a suitable probe for real-time cancer cell integrin expression detection.

In conclusion, we have designed a simple, robust graphene oxide (GO) based fluorescent biosensor for efficient, selective and real-time cancer cell surface marker integrin  $\alpha v \beta 3$  detection. We envision that this RGD–pyrene–GO biosensing system can be extended to evaluate other cell surface markers for cell surface marker imaging or ligand screening.

## Supplementary Material

Refer to Web version on PubMed Central for supplementary material.

## Notes and references

1. Rosi NL, Giljohann DA, Thaxton CS, Lytton-Jean AK, Han MS, Mirkin CA. *Science*. 2006; 312:1027–1030. [PubMed: 16709779]
2. Cai W, Shin DW, Chen K, Gheysens O, Cao Q, Wang SX, Gambhir SS, Chen X. *Nano Lett.* 2006; 6:669–676. [PubMed: 16608262]
3. Xie J, Jon S. *Theranostics*. 2012; 2:122–124. [PubMed: 22287992]
4. Zhen Z, Xie J. *Theranostics*. 2012; 2:45–54. [PubMed: 22272218]
5. Fu W, Nef C, Knopfmacher O, Tarasov A, Weiss M, Calame M, Schonenberger C. *Nano Lett.* 2011; 11:3597–3600. [PubMed: 21766793]
6. Rao CN, Sood AK, Subrahmanyam KS, Govindaraj A. *Angew. Chem., Int. Ed.* 2009; 48:7752–7777.
7. Liu Z, Robinson JT, Sun XM, Dai HJ. *J. Am. Chem. Soc.* 2008; 130:10876–10877. [PubMed: 18661992]
8. Sun XM, Liu Z, Welsher K, Robinson JT, Goodwin A, Zaric S, Dai HJ. *Nano Res.* 2008; 1:203–212. [PubMed: 20216934]
9. Li D, Song S, Fan C. *Acc. Chem. Res.* 43:631–641. [PubMed: 20222738]
10. Lu CH, Yang HH, Zhu CL, Chen X, Chen GN. *Angew. Chem., Int. Ed.* 2009; 48:4785–4787.
11. Chang H, Tang L, Wang Y, Jiang J, Li J. *Anal. Chem.* 2010; 82:2341–2346. [PubMed: 20180560]
12. Kim J, Cote LJ, Kim F, Huang J. *J. Am. Chem. Soc.* 2010; 132:260–267. [PubMed: 19961229]
13. Feng D, Zhang Y, Feng T, Shi W, Li X, Ma H. *Chem. Commun.* 2011; 47:10680–10682.
14. Wang H, Zhang Q, Chu X, Chen T, Ge J, Yu R. *Angew. Chem., Int. Ed.* 2011; 50:7065–7069.
15. Liu C, Wang Z, Jia H, Li Z. *Chem. Commun.* 2011; 47:4661–4663.
16. Wang Y, Li Z, Hu D, Lin CT, Li J, Lin Y. *J. Am. Chem. Soc.* 2010; 132:9274–9276. [PubMed: 20565095]
17. Feng T, Feng D, Shi W, Li X, Ma H. *Mol. BioSyst.* 2012; 8:1441–1445. [PubMed: 22334395]
18. Lu CH, Li J, Zhang XL, Zheng AX, Yang HH, Chen X, Chen GN. *Anal. Chem.* 2011; 83:7276–7282. [PubMed: 21859076]
19. Tcherkasskaya O, Davidson EA, Schmerr MJ, Orser CS. *Biotechnol. Lett.* 2005; 27:671–675. [PubMed: 15977076]
20. Balapanuru J, Yang JX, Xiao S, Bao Q, Jahan M, Polavarapu L, Wei J, Xu QH, Loh KP. *Angew. Chem., Int. Ed.* 2010; 49:6549–6553.
21. Xu Y, Bai H, Lu G, Li C, Shi G. *J. Am. Chem. Soc.* 2008; 130:5856–5857. [PubMed: 18399634]
22. Niu G, Chen X. *Theranostics*. 2011; 1:30–47. [PubMed: 21544229]
23. Gao J, Chen K, Xie R, Xie J, Yan Y, Cheng Z, Peng X, Chen X. *Bioconjugate Chem.* 2010; 21:604–609.
24. Wang H, Chen K, Cai W, Li Z, He L, Kashefi A, Chen X. *Mol. Cancer. Ther.* 2008; 7:1044–1053. [PubMed: 18483294]
25. Ye Y, Chen X. *Theranostics*. 2011; 1:102–126. [PubMed: 21546996]

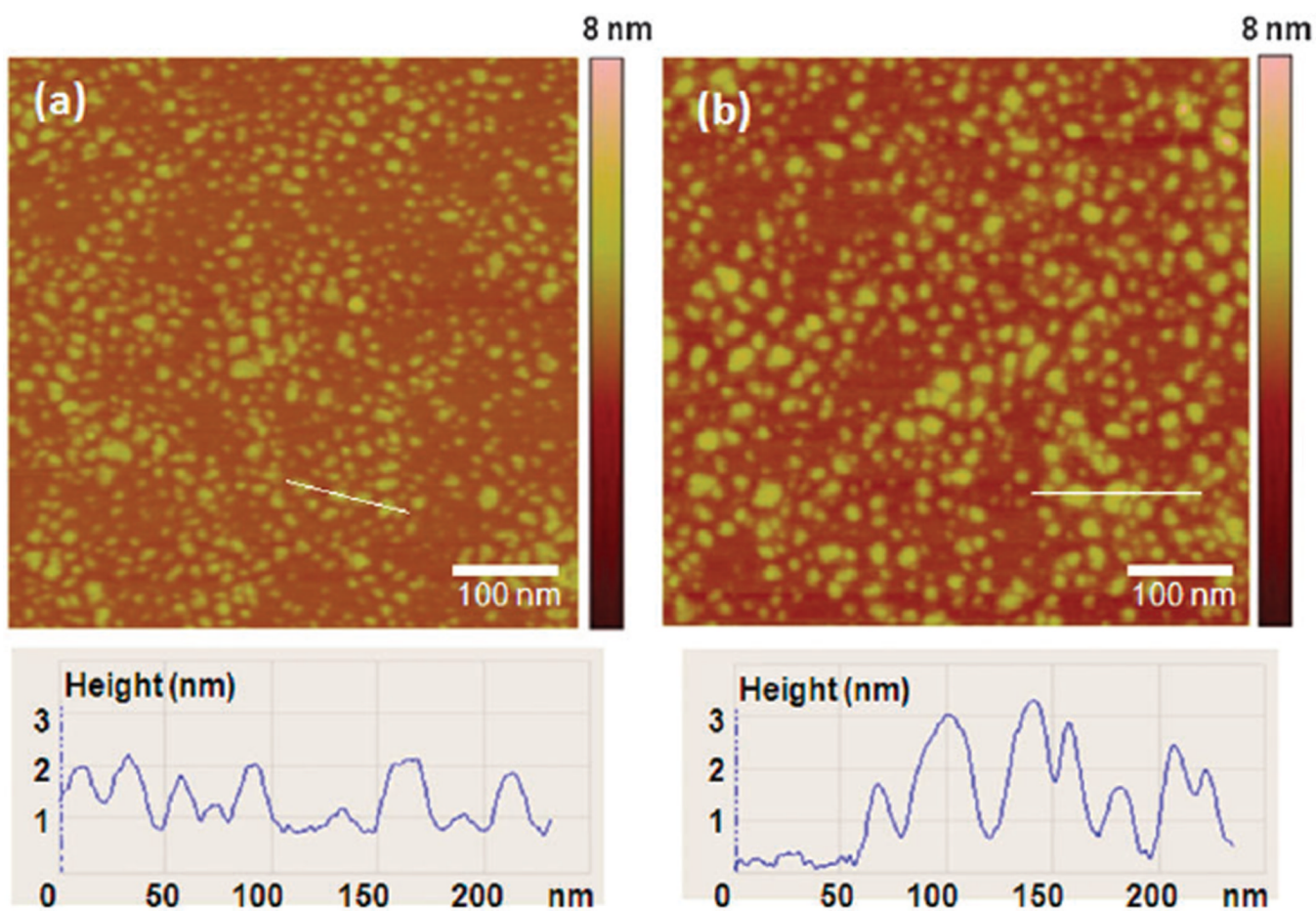


**Figure 1.**  
Atomic force microscopy (AFM) images of nanoscale graphene oxide before (a) and after (b) decorated with RGD-pyrene.

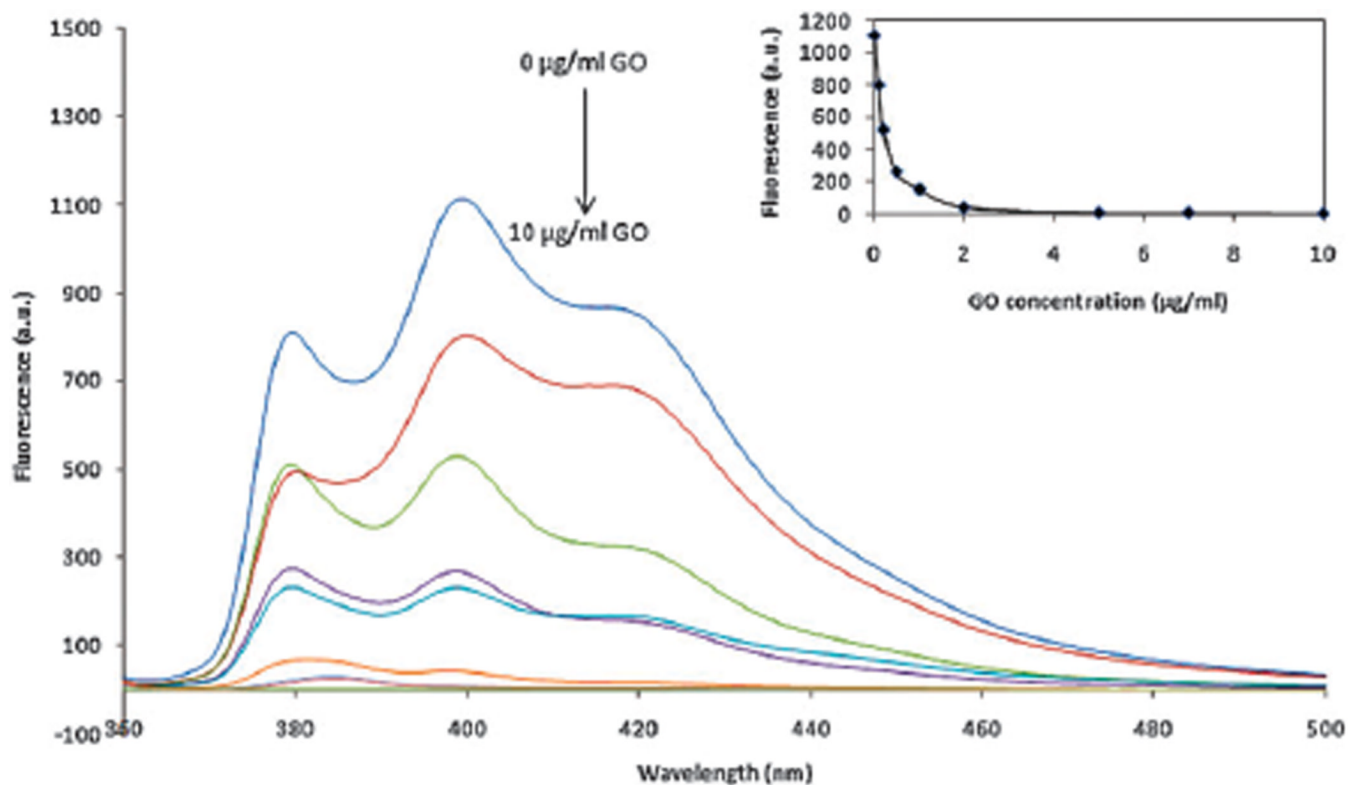


**Figure 2.** Fluorescence spectra of RGD-pyrene in the presence of various concentrations of GO (0, 0.1, 0.2, 0.4, 0.8, 1, 2, 5, 7, 10  $\mu\text{g mL}^{-1}$ ). Inset presents the plot of fluorescence intensity at 380 nm against the concentration of GO.  $\lambda_{\text{ex}}$ : 338 nm.

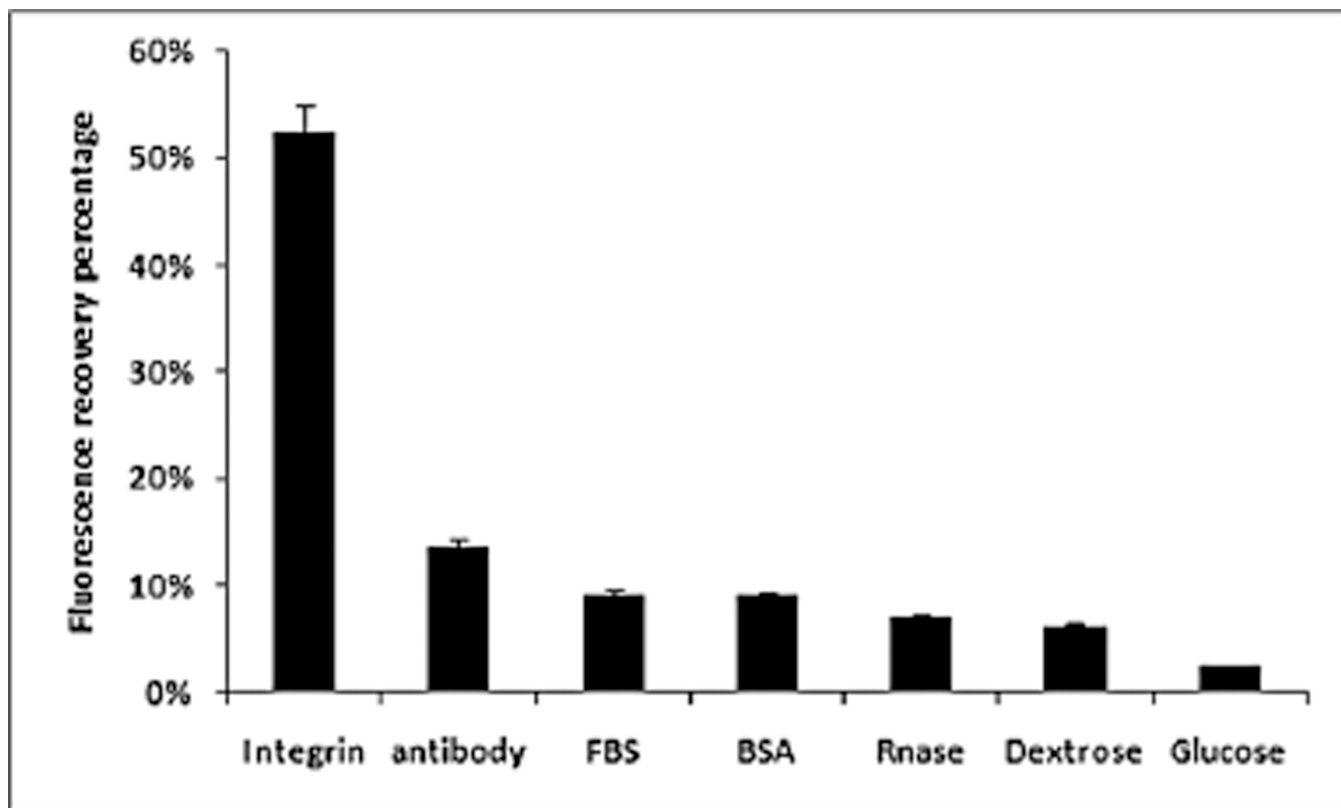
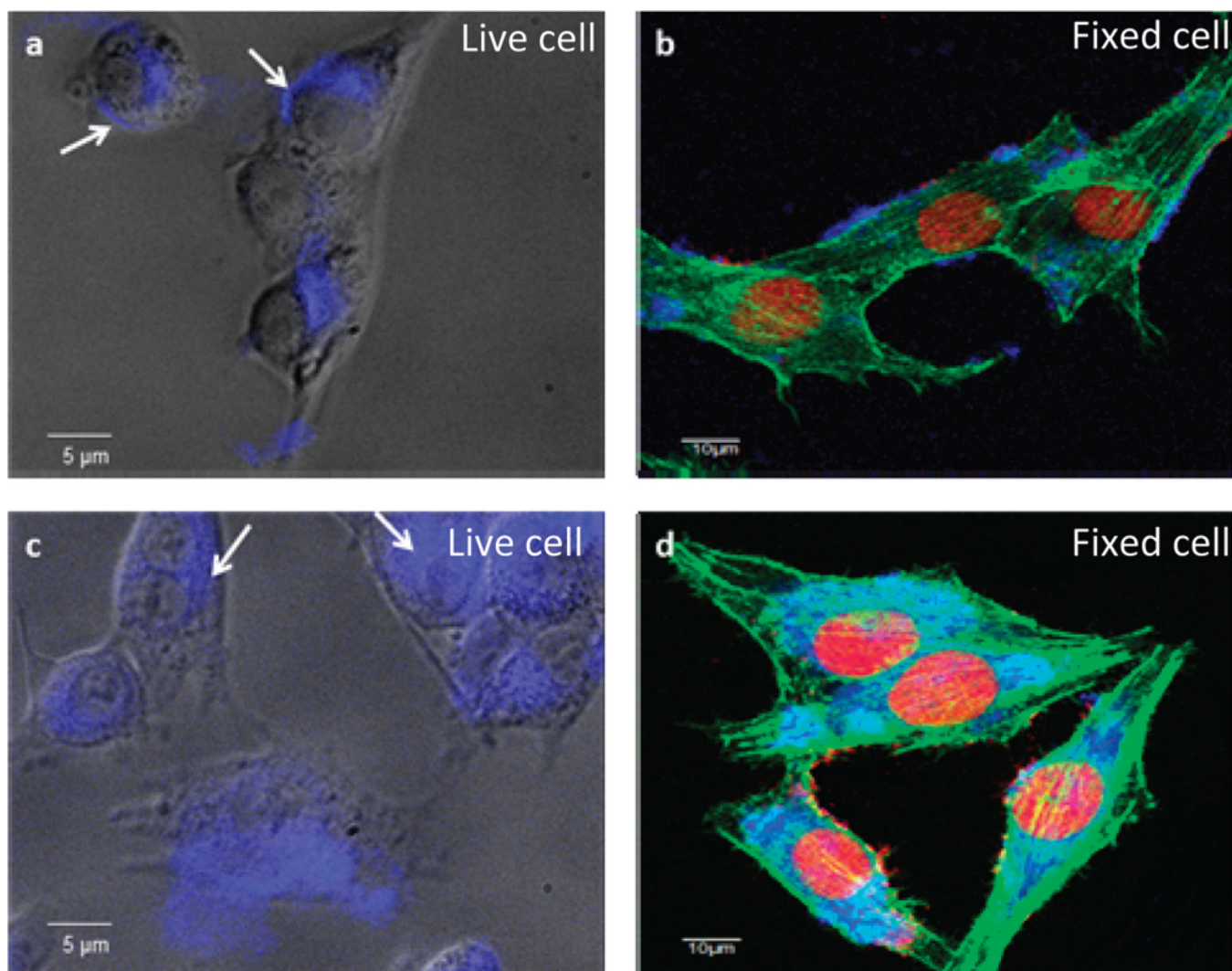
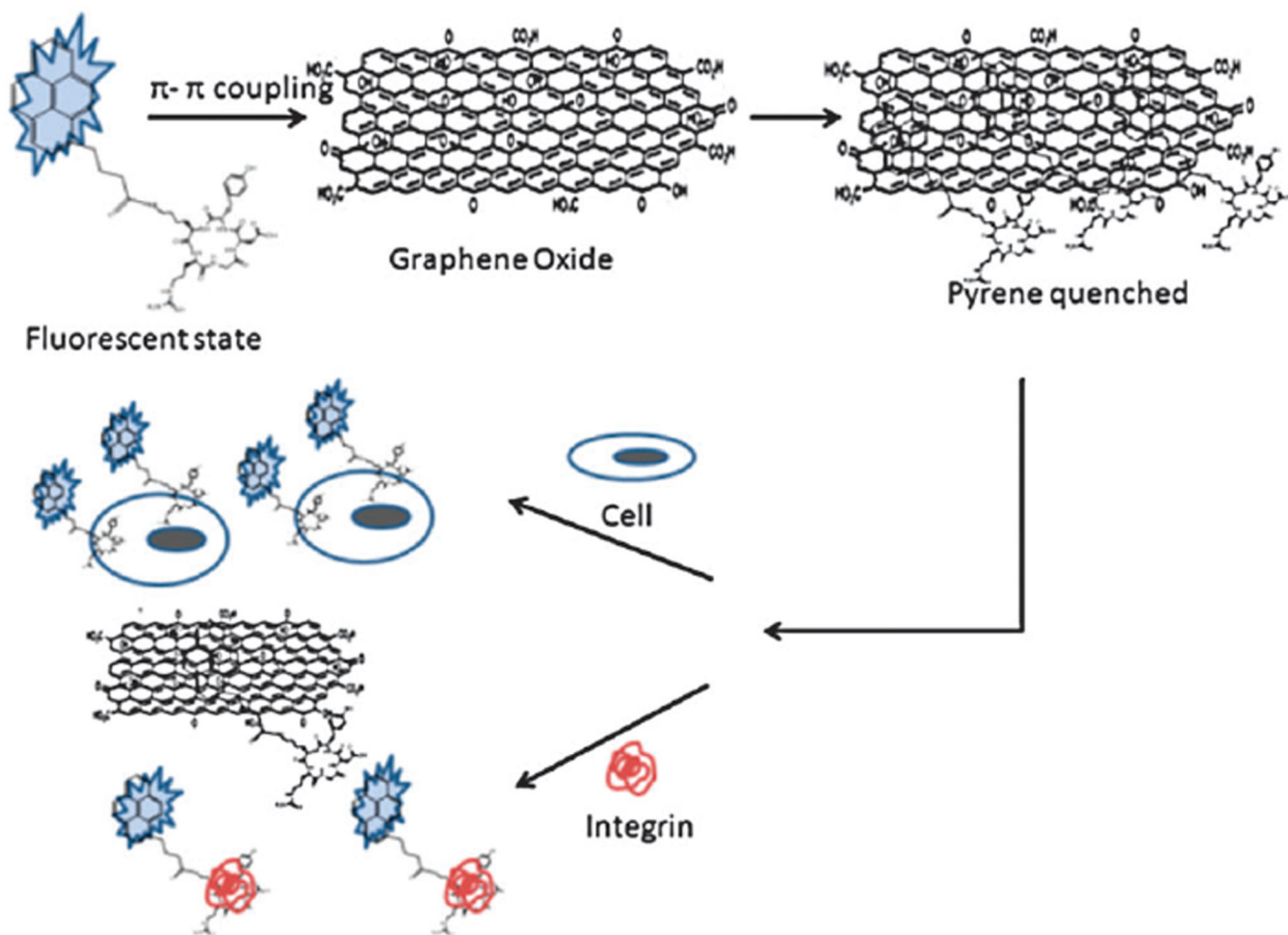


Figure 3.  
Specificity of integrin in recovering the fluorescence of the RGD–pyrene–GO complex.



**Figure 4.** Real-time *in situ* detection of breast cancer cell surface integrin expression by the RGD–pyrene–GO probe: (a) probe fluorescence recovery by live MDA-MB-435 cancer cells which overexpress integrin  $\alpha v\beta 3$  on the cell surface. The recovered fluorescence is mainly detected on the cell membrane as indicated by white arrows; (b) probe fluorescence recovery by MDA-MB-435 cancer cells followed by 4% formalin fixing; (c) equivalent concentration of free RGD–pyrene incubated with live MDA-MB-435 demonstrates significant endocytosis as indicated by white arrows; (d) equivalent concentration of RGD–pyrene incubated with MDA-MB-435 followed by 4% formalin fixing.





**Scheme 1.** Schematic illustration of RGD-pyrene interaction with GO to quench the fluorescence of pyrene, and the fluorescence recovery by introducing either integrin  $\alpha$ v $\beta$ 3 protein or integrin over-expressing cancer cells. Size is not in scale.